

# END-OF-LIFE DISPOSAL PARAMETRIC ANALYSIS IN CISLUNAR SPACE: EARTH-MOON $L_2$ ESCAPE NO-RETURN TRAJECTORIES

Mathilda Bolis<sup>(1)</sup>, Elisa Maria Alessi<sup>(2)</sup>, and Camilla Colombo<sup>(1)</sup>

<sup>(1)</sup>Department of Aerospace Science and Technology, Politecnico di Milano, Via La Masa 34, 20156 Milan, Italy, Email: mathilda.bolis@polimi.it, camilla.colombo@polimi.it

<sup>(2)</sup>Istituto di Matematica Applicata e Tecnologie Informatiche “Enrico Magenes”, Consiglio Nazionale delle Ricerche, Via Alfonso Corti 12, 20133 Milano, Italy, Email: em.alessi@mi.imati.cnr.it

## ABSTRACT

Recently, the importance of mitigating the proliferation of near-Earth space debris has been internationally recognised. As awareness is growing on space sustainability, similar principles as for the Earth orbital environment are being considered for cislunar space, with attention since the early stages of the mission design. Cislunar space offers great scientific opportunities but also poses challenges due to its highly non-linear dynamics. In this context, it is necessary to develop mitigation strategies before a space debris problem arises; the most effective of which is end-of-life disposal. Among the four strategies usually considered for disposal from periodic orbits, that of insertion into Earth-Moon  $L_2$  escape no-return trajectories is analysed here, thanks to an energetic approach combined with manifold dynamics. This leads to a cost analysis for selected orbits of some periodic orbit families, with results parametrised by various metrics, enabling the definition of an early-stage disposal cost map of cislunar space.

Keywords: Cislunar space; End-of-life; Escape no-return trajectories; Parametric analysis.

## 1. INTRODUCTION

In the last few years, the importance of mitigating the proliferation of near-Earth space debris has been internationally recognised. As the space sector has developed and satellite production has increased, especially with the introduction of CubeSats and large constellations, the awareness of the importance of space sustainability has also grown. At the same time, interest in cislunar space is rising: the Moon is seen as the next target for scientific and human exploration. This has been confirmed by the planning of major programs, such as Artemis [1], together with a lot of smaller, scientific missions. With the growing awareness of the need for space sustainability, the principles applied today to the overcrowded near-Earth space [2] are also being considered for the cislunar

region.

To address this increasing demand, the literature is proposing guidelines for End-of-Life (EoL) disposal in cislunar space to ensure its long-term sustainability [3][4]. In [4], ESA emphasises the importance of protecting Lunar orbits. To minimise the creation of space debris, it is recommended to avoid debris generation, to enhance space traffic coordination, and to implement precise disposal measures for spacecraft operating in the Earth-Moon (EM) region.

From the technical perspective, cislunar space offers significant opportunities for scientific and technological progress but also presents numerous challenges. Beyond the operational difficulties posed by the large distance from Earth [5], the dynamics of the region are strongly influenced by the gravitational attraction between the Moon, Earth and Sun, aggravated by the Moon’s irregular gravitational field, leading to highly non-linear behaviours. Also, “cislunar space” refers to a region extending from hyper-geostationary up to the Lagrangian points of the EM system [5]. Within this region, many different orbits can be identified, each with unique and complex characteristics: High Elliptical Orbits (HEOs), Lagrangian Point Orbits (LPOs), quasi-satellite orbits, and others.

Considering all of this, a space debris problem, similar to that observed in near-Earth space, could also develop in the EM region, intensified by its highly non-linear dynamics. It is essential to develop mitigation strategies, the most effective being well-designed EoL disposal for missions operating in that area.

According to ESA [4], disposal plans for spacecraft operating in lunar orbits shall include one of the following strategies “in order of preference: heliocentric disposal, Lunar impact, Earth re-entry, or a Lunar graveyard orbit.” The choice of one of these strategies must be justified by orbit propagation analyses. Also, in the case of disposal towards a Lunar graveyard orbit, it must be guaranteed that the orbit remains bounded for at least 100 years. In general, disposal trajectories should be assessed over a minimum of 100 years to determine the probability of Earth re-entry or Lunar impact, including the associated impact zones.

Heliocentric disposal consists of designing a trajectory

that moves from a periodic orbit in the EM system to a region outside  $L_1$  or, preferably,  $L_2$  of the Sun-Earth (SE) system. In [6], an energetic approach based on three-body dynamics is applied to LPOs in SE- $L_2$  such that, after the disposal trajectory passes through SE- $L_2$ , the Zero Velocity Curves (ZVCs) are closed to prevent the spacecraft from re-entering the SE vicinity. This strategy is also applied in [7], [8] and [9] to the EoL design for Herschel, SOHO and Gaia, operating on LPOs in SE- $L_2$ , where disposal trajectories are also validated in an  $n$ -body model. In [10], the effect of solar radiation pressure is used to derive low-cost solutions, implemented via solar sails. In the EM system, this strategy was applied by [11] to the NRHO chosen as a baseline for the Lunar Gateway.

In this paper, a preliminary parametric disposal cost-analysis for EM- $L_2$  escape no-return trajectories is presented, where no-return refers to trajectories that theoretically do not return inside the cislunar region after the disposal phase. Orbits from the Halo and Lyapunov families around  $L_1$  and  $L_2$  are selected, and the disposal cost is calculated for these orbits as the phase angle and the time spent by the spacecraft on the manifold before the disposal phase vary. The EoL phase is modelled as a two-impulse manoeuvre: the first impulse inserts the satellite into the corresponding LPO unstable manifold, while the second one causes the EM system's ZVCs to close, preventing the satellite from returning to the inner region of cislunar space. Some disposal trajectories are verified to remain outside the system for 100 years, both in a three-body dynamics and in an  $n$ -body model.

## 2. MODELLING TECHNIQUES

### 2.1. Circular Restricted Three Body Problem

The Circular Restricted Three-Body Problem (CR3BP) [12] describes the motion of a massless object subject to the gravitational influence of two major bodies, e.g. the Earth and the Moon, orbiting in a circular motion around their common centre of mass. The position and velocity of the massless object are defined as  $\mathbf{r} = [r_x, r_y, r_z]$  and  $\mathbf{v} = [v_x, v_y, v_z]$ . They are found in a rotating reference frame, where the primaries are located along the  $x$ -axis, defined as the line connecting them, with the origin in their centre of mass and the positive direction toward the smaller primary. The  $z$ -axis is perpendicular to the primaries' orbital plane, and the  $y$ -axis completes the right-handed tern. The Equations of Motion (EoMs) characterising the CR3BP are:

$$\begin{cases} \dot{\mathbf{r}} = \mathbf{v} \\ \dot{\mathbf{v}} = 2 \begin{bmatrix} v_y \\ -v_x \\ 0 \end{bmatrix} + \nabla_{\mathbf{r}} U \end{cases} \quad (1)$$

where the potential-like function  $U$  is defined as:

$$U(\mathbf{r}) = \frac{1}{2}(r_x^2 + r_y^2) + \frac{1-\mu}{r_1} + \frac{\mu}{r_2} + \frac{1}{2}\mu(1-\mu) \quad (2)$$

The parameter  $\mu$  is the dimensionless EM system gravitational constant, equal to 0.01215;  $r_1$  and  $r_2$  are the distances between the third body and each of the primaries, respectively. Since the major primary is at  $x = -\mu$  and the minor one at  $x = 1 - \mu$ ,  $r_1$  and  $r_2$  are defined as:

$$r_1 = ((r_x + \mu)^2 + r_y^2 + r_z^2)^{1/2} \quad (3)$$

$$r_2 = ((r_x - 1 + \mu)^2 + r_y^2 + r_z^2)^{1/2} \quad (4)$$

All quantities are considered dimensionless: lengths are scaled to the mean EM distance and times so that the mean motion of the rotating reference frame is equal to 1. Accordingly, dimensionless lengths are denoted by the unit  $ndL$ , non-dimensional length, and dimensionless times by the unit  $ndT$ , non-dimensional time. In CR3BP, only one integral of motion can be defined. A version of this integral, known as Jacobi Constant (JC), is as follows:

$$JC(\mathbf{r}, \mathbf{v}) = 2\bar{U}(\mathbf{r}) - \|\mathbf{v}\|^2 \quad (5)$$

where

$$\bar{U}(\mathbf{r}) = \frac{1}{2}(r_x^2 + r_y^2) + \frac{(1-\mu)}{r_1} + \frac{\mu}{r_2} \quad (6)$$

The  $JC$  is a function of the state of the spacecraft and it can be related to an energy-like constant. The CR3BP is a Hamiltonian system and, when computing its EoMs using a Hamiltonian approach, a constant similar to the total mechanical energy is defined, such that  $E = -JC/2$ . By this definition, an increase in  $JC$  corresponds to a decrease in system energy and vice versa.

### 2.2. Libration points and zero velocity curves

The CR3BP has five equilibrium points, the Libration or Lagrange points  $L_1 - L_5$ . Of these,  $L_1 - L_3$  lie on the  $x$ -axis of the rotating reference frame and are called collinear Lagrange points. Instead,  $L_4$  and  $L_5$  form the vertices of an equilateral triangle with the major primary and are called triangular Lagrange points.

The possible motion of a massless particle can be classified according to its energy. In the spatial CR3BP, for a fixed energy level  $E_0$ , a five-dimensional energy surface embedded in a six-dimensional phase space can be

defined. The regions of possible motion for a massless object with energy  $E_0$  in a system with gravitational constant  $\mu$  are defined by projecting the energy surface into position space in the rotating frame. This region is historically known as the Hill region and its boundaries as ZVCs, which are identified as the locus of points where the kinetic energy of the massless particle equals zero. Considering a fixed  $JC$  level,  $JC_0$ , which corresponds to the fixed energy level  $E_0$ , and since  $JC(\mathbf{r}, \mathbf{v})$  is defined as in Equation (5), we find that  $2\bar{U}(\mathbf{r}) \geq JC_0$ . The boundary condition  $2\bar{U}(\mathbf{r}) = JC_0$  is required for  $\mathbf{v} = 0$  and identifies the ZVCs. Instead, regions in space where the inequality does not hold are called forbidden regions, i.e. areas where the motion of the third body is not allowed. If we consider the motion restricted to the plane of the primaries, the ZVCs result in a curve that forms a barrier that the massless third body can not cross in the planar position space. In Figure 1, the location of the five Libration points of the EM system is shown, together with the planar ZVCs as a function of the  $JC$  considered.

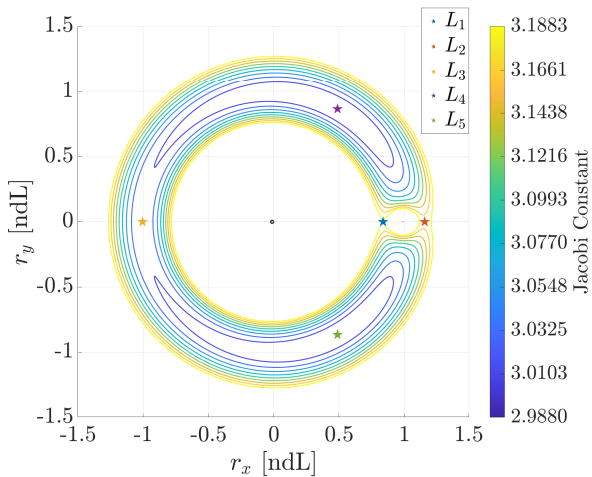


Figure 1: Libration points and ZVCs as a function of the Jacobi Constant in the EM system.

In Figure 2, ZVCs are shown for three different increasing values of  $JC$ , and forbidden regions are highlighted. Near the Moon, a bottleneck region is present and closes as the  $JC$  of the system increases, i.e. as the energy belonging to the massless third body decreases. When the  $JC$  of a trajectory is equal to that of  $L_2$ ,  $JC_{L_2}$ , the ZVCs of the EM system close. For a particle with  $JC > JC_{L_2}$  that moves outside the forbidden area, it is not possible to return to the interior region without changing its energy, e.g. performing manoeuvres. Conversely, a particle in the inner region must reach a certain energy for the bottleneck region to open and reach the outer region.

### 2.3. Periodic orbits

In a three-body system, several families of periodic orbits can be identified [13]. In this paper, a subset of such orbits is selected as the starting point for the analysis. Peri-

odic orbits are generated thanks to a Newton-like differential correction method. Periodicity and orthogonality are enforced, which means that

- periodic orbits must be symmetric about the  $xz$ -plane (or the  $x$ -axis in the planar case) and intersect this plane perpendicularly,
- a state  $\mathbf{x} = [\mathbf{r}, \mathbf{v}]$  must repeat itself after one period.

These properties enable a given initial state to be linked to an ideal final state, the desired characteristics of which are known, and the differential correction algorithm allows for the adjustment of the initial state so that the final one is as desired [14]. This leads to the definition of initial conditions generating a periodic orbit when propagated in CR3BP over a period. After finding a first orbit belonging to a certain family, the procedure is iterated to find other members of that same family. Knowing the first solution obtained, initial guesses are derived thanks to continuation methods, such as the natural parameter continuation or the pseudo arclength method.

Numerous families of periodic orbits bifurcating from Libration points can be defined in the EM system. The analysis presented here considers four families of LPOs with similar characteristics: the Halo and Lyapunov families in  $L_1$  and  $L_2$ . For Halo orbits, the southern branch of the family is considered. These families were chosen for their relevance to future missions and for the linear instability that characterises almost all their members: as it will be detailed in Section 3, the method used to design EoL solutions is based on the inherent instability of these orbits. The orbits considered in the analysis are 12 in total, 3 for each of the 4 families considered, and are represented in Figure 4 and Figure 3.

In the Figures, the blue dot represents  $L_1$ , and the red dot represents  $L_2$ . The orbits considered are represented both as a function of the phase angle and the distance from the Moon. The phase angle, which is a relevant parameter also in the analysis presented later, is defined as:

$$\theta = \frac{2\pi t}{T} \quad (7)$$

It is interesting to note that, for the Halo orbits selected, the evolution of the distance from the Moon follows a pattern similar to that of the phase angle. In the case considered in this paper, when  $\theta$  approaches  $180^\circ$ , the distance between the orbit and the Moon reaches its minimum, while it is maximised when the phase angle is  $0^\circ$ . A similar behaviour is observed in Lyapunov orbits in  $L_1$ , although the relationship between these two variables appears slightly different for orbits far from the Lagrangian point generating them, as the distance from the Moon decreases slightly at  $0^\circ$  before reaching its maximum around  $90^\circ$ . The minimum distance is reached, as in the spatial case, for  $\theta = 180^\circ$ . For Lyapunov orbits in  $L_2$ , the phase angle trend as a function of the distance from the Moon is shifted by  $180^\circ$  compared to what is

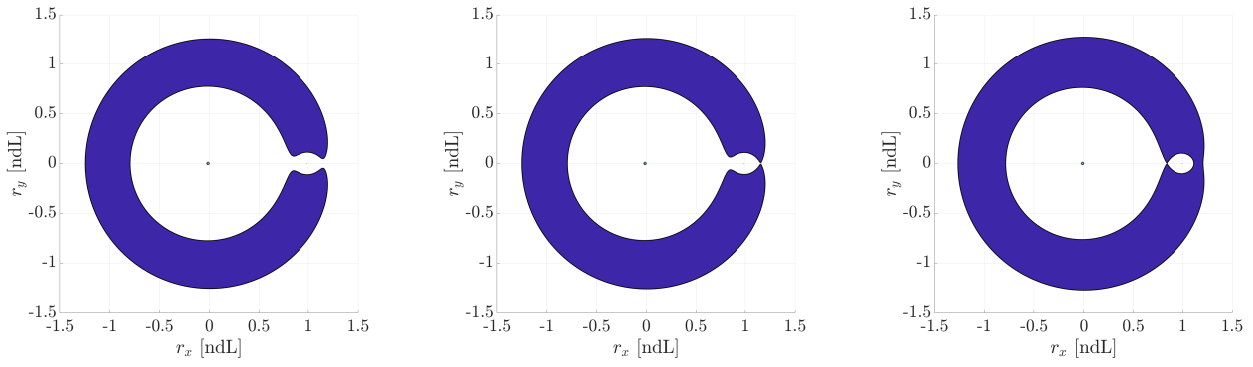


Figure 2: ZVCs in the EM system for different values of Jacobi Constant. From left to right:  $JC = 3.1671$ ;  $JC = 3.1721$ , corresponding to the Jacobi Constant relative to  $L_2$ ;  $JC = 3.1883$ , corresponding to the Jacobi Constant relative to  $L_1$ .

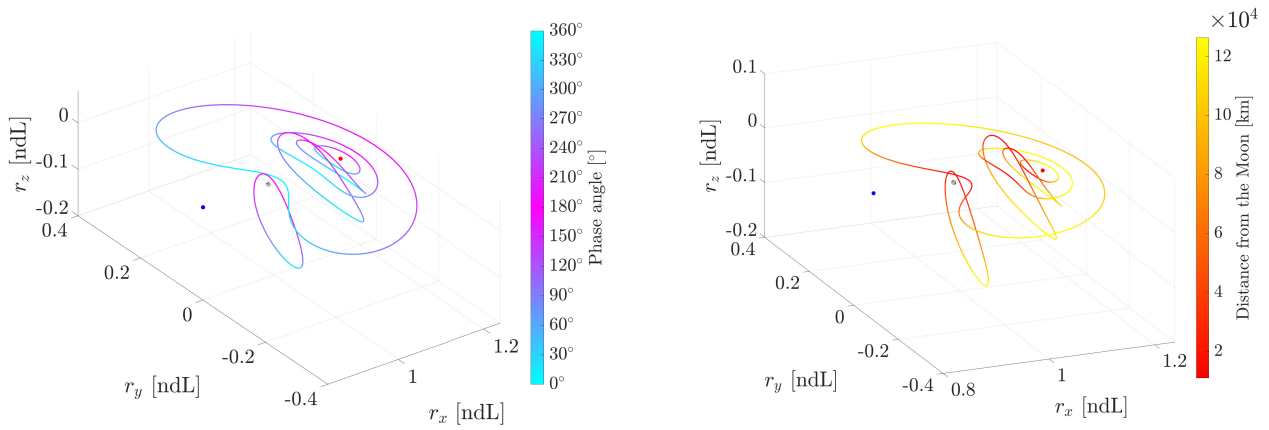


Figure 3: LPOs around EM- $L_2$  selected for the analysis, as a function of the phase angle and the distance from the Moon.

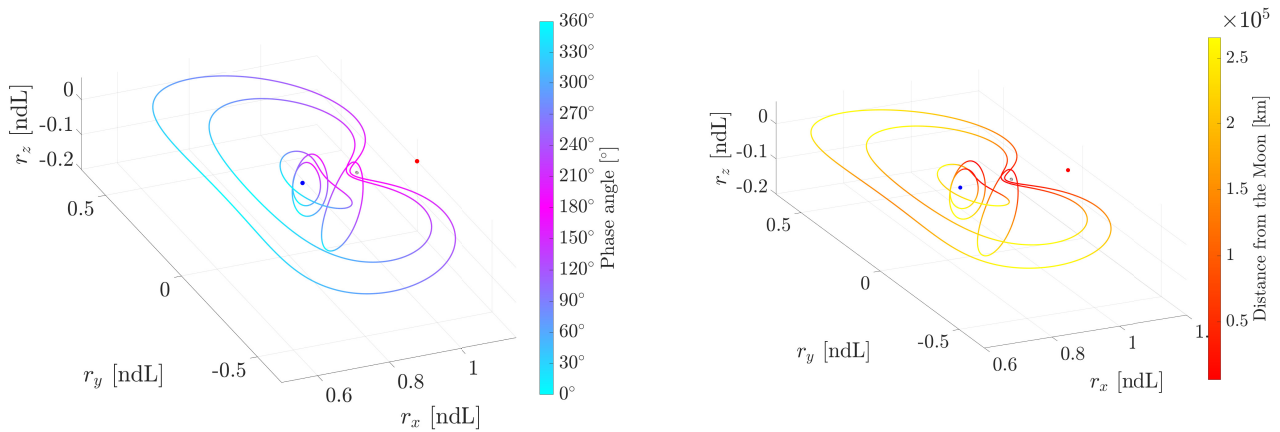


Figure 4: LPOs around EM- $L_1$  selected for the analysis, as a function of the phase angle and the distance from the Moon.

observed for Lyapunov orbits in  $L_1$ . This is simply due to the choice made for the definition of a point such that  $\theta = 0^\circ$ .

In Table 1, some other characteristics of the LPOs considered are listed. For each LPO, three parameters are recorded: the  $JC$  of the periodic orbit, which remains constant along the entire trajectory since no external perturbations to CR3BP are considered; the Stability Index (SI) of the periodic orbits, which defines their linear stability; and  $r_p$ , the perilune radius, defined as the minimum distance between the orbit and the Moon along one orbital period. Note that periodic orbits are considered stable if with an  $SI < 1$  [15].

Table 1: Some relevant parameters of the LPOs considered.

Orbit type	$JC$	$SI$	$r_p$ [km]
Halo $L_2$	3.1383	473.55	48813.79
	3.0988	210.03	42870.44
	3.0289	1.69	7302.42
Lyapunov $L_2$	3.1612	659.02	54880.68
	3.1161	426.52	39526.96
	2.9867	88.66	11025.32
Halo $L_1$	3.1525	800.62	49184.21
	3.1239	458.88	46790.89
	3.0025	2.03	9705.18
Lyapunov $L_1$	3.0804	442.29	32383.20
	2.9370	58.97	9264.38
	2.8968	54.76	6125.12

## 2.4. Ephemeris model

The CR3BP is a good approximation of the dynamics of a particle moving in cislunar space. However, to verify the effectiveness of the disposal trajectories found, it is worth assessing what the effect of the gravitational influence of celestial bodies other than the Earth and Moon might be in the system. An  $n$ -body dynamical model is implemented [16], based on celestial bodies' ephemerides retrieved via the DE442 kernel of NASA's SPICE toolkit [17]. In addition to the Earth and the Moon, the influence of the Sun has the greatest impact on the system. However, for a comprehensive analysis, the Earth, Moon, Sun, Mercury, Venus, Mars and Jupiter are included in the dynamical model, resulting in an 8-body model (7 celestial bodies plus the spacecraft). Since this is a preliminary study, March 8, 2025, at 22:31 is selected as the starting date for the propagation. This choice is made because, on that date, the position of the Moon is very similar to what it would be in the approximation used in the EM rotating frame, which means we are in a condition such that the EM distance is similar to its mean value. The EoMs for the  $n$ -body model in an Earth-centred J2000 inertial reference frame are governed by the evolution of the inertial position vector  $\mathbf{s} = [s_x, s_y, s_z]$ , defined as the distance

between the spacecraft and the Earth in the inertial reference frame:

$$\ddot{\mathbf{s}} = -\frac{\mu_1}{\|\mathbf{s}\|^3}\mathbf{s} - \sum_{j=2}^n \mu_j \left( \frac{\mathbf{d}_j}{\|\mathbf{d}_j\|^3} + \frac{\boldsymbol{\rho}_j}{\|\boldsymbol{\rho}_j\|^3} \right) \quad (8)$$

where  $\mu_j$  are the standard gravitational constants of the  $j$ -th bodies. Since the dynamics are propagated in an Earth-centred reference frame, the subscript 1 refers to Earth. Earth is chosen as the centre of the reference system because the  $n$ -body model will only be used to validate that the spacecraft, after disposal, does not re-enter cislunar space. In this context, we are working within a system whose centre can be roughly defined as Earth. The vectors  $\boldsymbol{\rho}_j$  and  $\mathbf{d}_j$  are respectively defined as the positions of other solar system bodies with respect to the Earth and as the positions of the spacecraft with respect to each perturbing body, resulting in  $\mathbf{d}_j = \mathbf{s} - \boldsymbol{\rho}_j$ .

For propagation with the  $n$ -body dynamics, the state of a point in the EM rotating frame must be properly scaled and transformed into an Earth-centred inertial frame. To do so:

$$\mathbf{s} = \mathbf{R}(\mathbf{r} - \mathbf{p}_{E_{rot}}) \quad (9)$$

$$\dot{\mathbf{s}} = \mathbf{R}\mathbf{v} + \boldsymbol{\omega}_{rot} \times \mathbf{s} \quad (10)$$

where  $\mathbf{p}_{E_{rot}}$  is the position of the Earth in the EM rotating frame,  $\boldsymbol{\omega}_{rot}$  is the angular velocity of the EM rotating frame and  $\mathbf{R}$  is the time-dependent rotation matrix that connects the two frames. Then,  $\mathbf{s}$  and  $\dot{\mathbf{s}}$  are appropriately scaled.

## 3. ESCAPE NO-RETURN DISPOSAL TRAJECTORIES

The objective of the escape no-return disposal trajectories is to move a spacecraft from an LPO defined in the EM CR3BP to the external regions of cislunar space. This is achieved by designing two-impulse disposal trajectories, closing the ZVCs once outside EM- $L_2$  to prevent the spacecraft from returning to the EM vicinity. Simulations will be performed in CR3BP, and then validation will be carried out with an  $n$ -body model for some of the disposal trajectories to remain outside cislunar space for 100 years. It is important to specify that, according to the lunar space debris mitigation guidelines defined in, for example, [4], the disposal phase is completed only when the spacecraft is in the exterior region of the SE system, not just the EM one. However, it is considered worthwhile to study the dynamics that characterise  $L_2$  escape no-return trajectories to better understand which parameters influence the disposal dynamics and costs. In a second phase, the analysis will be extended to trajectories escaping from SE  $L_2$  that do not re-enter the inner region

of the SE system for 100 years.  $L_2$  escape no-return trajectories are designed following the schema illustrated in Figure 5.

The first impulse is given in the unstable manifold direction. Manifolds are sets of trajectories that asymptotically approach or depart from an LPO in CR3BP, in forward time. Their directions can be estimated numerically thanks to the State Transition Matrix (STM) of an LPO. First, the eigenvalues and eigenvectors of the monodromy matrix, i.e. the STM evaluated at a time equal to one orbital period, are evaluated. In the spatial CR3BP, the STM has six eigenvalues. As LPOs are considered, a pair of eigenvalues is always equal to unity since energy along unperturbed trajectories in CR3BP is conserved. Among the remaining two pairs, one consists of complex conjugate eigenvalues, while the other consists of real and reciprocal eigenvalues. This pair,  $\lambda^{s,u}$ , will be such that  $|\lambda^s| < 1$  and  $|\lambda^u| > 1$ . The eigenvalue  $\lambda^u$  is associated with the eigenvector  $\Lambda^u(\theta_0)$  which is tangent to the direction that asymptotically leaves the LPO, i.e. the unstable manifold. This direction is a function of the phase angle of the orbit. When the eigenvector is computed from the monodromy matrix, it corresponds to the direction of the unstable manifold for  $\theta = 0^\circ$ , equivalent to  $t = t_0$ . To compute the direction of the unstable manifold at a generic time  $t$ , and so at the generic phase angle  $\theta$ , it is necessary to know that:

$$\Lambda^u(\theta) = \Phi(t_0, t)\Lambda^u(\theta_0) \quad (11)$$

where  $\Phi(t_0, t)$  and  $\theta$  are the STM and the phase angle evaluated at time  $t$  respectively. Thanks to the STM, the unstable manifold directions are mapped along the overall LPO. The directions are then normalised such that:

$$\hat{\Lambda}^u(\theta) = \frac{\Lambda^u(\theta)}{\|\Lambda^u(\theta)\|} \quad (12)$$

To approximate an initial condition on the unstable manifold, a perturbation is given to a state on an LPO along the normalised direction found:

$$\mathbf{x}_0^u(\theta) = \mathbf{x}_0(\theta) \pm \varepsilon \hat{\Lambda}^u(\theta) \quad (13)$$

The perturbation  $\varepsilon$  needs to be sufficiently large to enable the trajectory to depart from the LPO naturally, yet sufficiently small to avoid violating linearity. In the SE system, this value is typically set to result in a position displacement of 200 km [6]. When scaled for the EM system, this corresponds to a position displacement of 250 m, which results in a perturbation  $\varepsilon$  of the order of magnitude of  $10^{-7}$  when appropriately scaled. The value of  $\Delta v_1$  is computed as the norm of the velocity variation necessary to insert the spacecraft in the manifold.

The sign of  $\varepsilon$  influences which branch of the unstable manifold is considered. The unstable manifold splits into two branches, the first one heading towards the smaller

primary, and the second one away from it. Given the application analysed, the branch heading away from the Moon must be selected. It has been noted that, along a single LPO family, the branch heading away from the Moon is not always characterised by a positive or negative value of  $\varepsilon$ , meaning that, as  $\theta$  varies along an orbit, the sign of  $\varepsilon$  that leads the unstable manifold away from the smaller primary is always the same, either positive or negative, but it is not always the same along an entire family of orbits. Since we do not know before the analysis if the branch we are interested in is defined by a positive or a negative perturbation, both branches of the manifold are initially propagated for 6 months. The manifold branch is selected as the one directed toward  $L_2$ . Propagation is performed thanks to a variable-step, variable-order Adams-Bashforth-Moulton predictor-corrector solver of orders 1 to 13. Relative tolerances are set to  $2.22045 \cdot 10^{-14}$ , absolute tolerances to  $10^{-16}$ .

Once the proper sign of  $\varepsilon$  is found, the selected branch of the unstable manifold is propagated forward for up to 6 months. As  $\theta$  varies, trajectories that impact the Moon or Earth before exiting EM- $L_2$  are identified and considered infeasible as a disposal option. The same applies to trajectories that remain in the inner region of cislunar space for the entire 6 month time span, since it is preferred to rapidly exit from EM- $L_2$ . The cislunar space is characterised by highly non-linear dynamics and, as a result, trajectories orbiting the inner region of the ZVCs for a long period before leaving it are not a good option for EoL disposal, as the probability of an uncontrolled impact on Earth or the Moon is very high. All remaining trajectories are considered for the following analysis.

Once a condition is reached such that the position of the spacecraft on the trajectory is beyond EM- $L_2$ , a second impulse must be given to change its energy and close the ZVCs of the EM system. To do so, it is sufficient to modify the  $JC$  of the trajectory, from  $JC'$  to  $JC''$ , such that  $JC'' \geq JC_{L_2}$  [7][8] [9]. If this condition is met, the ZVCs of the EM system close, as also shown by Figure 2, and it would be impossible for an object outside them to return to their inner region, at least with a CR3BP dynamics. This strategy is referred to as *energetic approach*: the change in the energy of the system will result in a change in the velocity of the particle, i.e., a manoeuvre. Since the  $JC$  of a particle is defined as in Equation (5) and its position is not a parameter that can be varied, the relationship between  $JC'$  and  $JC''$ , where the superscript ' refers to the trajectory state immediately before the manoeuvre and '' to the state immediately following it, is:

$$JC'' = JC' + \|\mathbf{v}'\| - \|\mathbf{v}''\| \quad (14)$$

Let's consider a manoeuvre tangent to the velocity direction, being  $\mathbf{v}'' = \mathbf{v}' + \Delta v_2$ . Substituting this relationship in Equation (14) and considering the limit case such that  $JC'' = JC_{L_2}$ , it can be found that:

$$\Delta v_2 = -\|\mathbf{v}'\| \pm \sqrt{\|\mathbf{v}'\|^2 - \Delta JC} \quad (15)$$

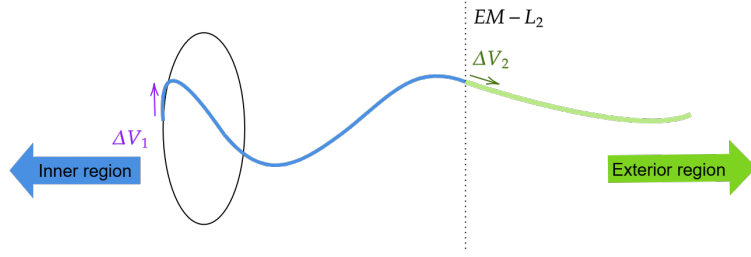


Figure 5: EM  $L_2$  escape no-return disposal trajectories, schematic representation.

where  $\Delta JC = JC_{L_2} - JC'$ . The minus sign in the equation is not considered in this analysis, as it usually relates to retrograde orbits. Note that the manoeuvre contributes to increasing the  $JC$  of the trajectory, i.e. decreasing its energy. Consequently, the manoeuvre to close the ZVC is tangent to the velocity direction but has the opposite sign, which means that all  $\Delta v_2$  computed thanks to Equation (15) will be negative.

#### 4. RESULTS

The analysis described in the previous Section is applied to all orbits defined in Table 1. The first orbit considered belongs to the Halo family at  $L_2$ , and is reported as first in the Table. In Figure 6, the results of the cost analysis, in terms of total  $\Delta V$  budget for the two manoeuvres, are shown.

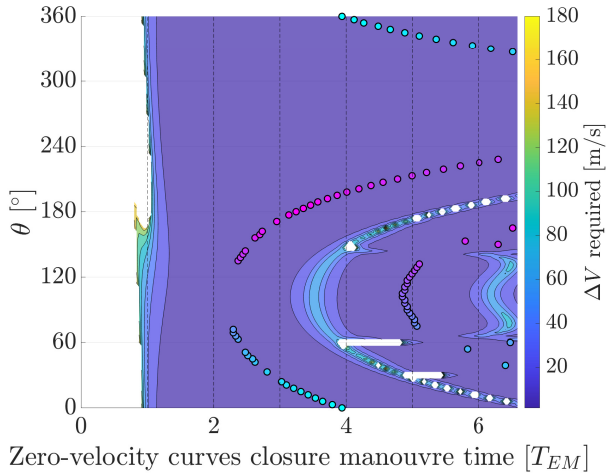


Figure 6: Disposal  $\Delta V$  as a function of the phase angle and the time the satellite spends on the manifold before performing the second disposal manoeuvre. Halo  $L_2$ ,  $JC = 3.1383$ .

To get a comprehensive view of the cost evolution, the graph in Figure 6 is reproduced as a three-dimensional surface in Figure 7.

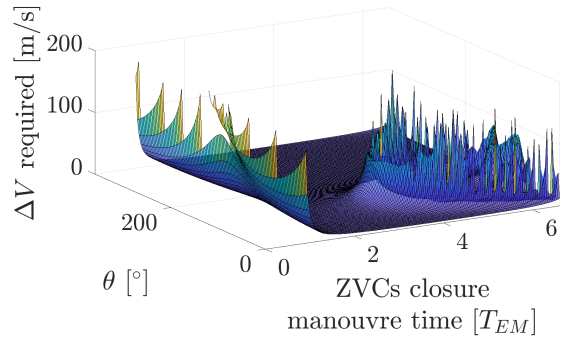


Figure 7: Disposal  $\Delta V$  as a function of the phase angle and the time the satellite spends on the manifold before performing the second disposal manoeuvre - 3D view. Halo in  $L_2$ ,  $JC = 3.1383$ .

The total cost of the disposal manoeuvre is reported as a function of the phase angle  $\theta$ , which varies along the orbit from  $0^\circ$  to  $360^\circ$  (see Figure 3), and the time spent by the spacecraft on the manifold before the ZVCs closure manoeuvre is applied,  $t_{\Delta v_2}$ . The value  $t = 0$  corresponds to the time when the spacecraft is injected into the unstable manifold. The maximum allowed time of flight on the manifold is 6 months. The parameter  $t_{\Delta v_2}$  is significant for the analysis because, although the second disposal manoeuvre can theoretically be performed just after exiting  $L_2$ , in some cases it may be useful to allow the spacecraft to remain on the manifold for some time before executing it. The value of  $t_{\Delta v_2}$ , on the  $x$ -axis of Figure 6, is parametrised as a function of the EM period, equal to 27.32 days. The coloured dots in Figure 6 represent the minimum  $\Delta V$  conditions for each phase angle considered. The colour map used for the dots is not related to the one representing the evolution of  $\Delta V$  and it is instead associated with the corresponding phase angle, as in Figure 3 and Figure 4. For phase angles where no minimum  $\Delta V$  dot is present in the Figure, the minimum  $\Delta V$  is found in the correspondence of a ZVCs closure time equal to 6 months. This could mean that, for such values of  $\theta$ , a lower  $\Delta V$  could be found if a longer time spent by the spacecraft along the manifold is considered. Consequently, these conditions are not reported in the Figures, as not of interest for the following analysis.

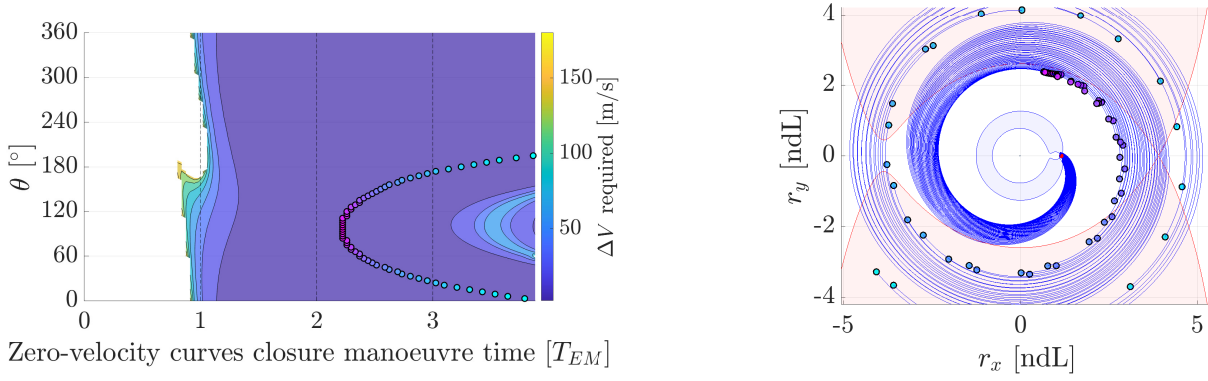


Figure 8: Left: Disposal  $\Delta V$  as a function of the phase angle and the time the satellite spends on the manifold before performing the second disposal manoeuvre - Reduced total time considered. Right: Trajectories corresponding to minimum disposal  $\Delta V$  conditions in the EM rotating frame. Halo  $L_2$ ,  $JC = 3.1383$ .

As shown in Figure 6, disposal cannot be performed for low values of  $t_{\Delta v_2}$ . These cases correspond to conditions such that the spacecraft is still in the inner region of the ZVCs of  $L_2$ . Once the manifold trajectories reach  $L_2$ , disposal is possible but costly: after a short time, the same manoeuvres can be carried out with  $\Delta V$ s lower by even an order of magnitude. In some cases, also for large values of  $t_{\Delta v_2}$ , some areas of the Figures are empty. These areas correspond to conditions such that the manifold, previously outside the ZVCs of  $L_2$ , temporarily re-enters them. Consequently, disposal under these conditions is not feasible.

From Figure 7, it can be observed that as  $\theta$  varies, a region of minimum  $\Delta V$  already appears after the satellite has spent approximately two EM periods on the manifold. If it is necessary to complete the disposal quickly, waiting to reach just this condition could save a significant amount of fuel, at the cost of a  $t_{\Delta v_2}$  which is only slightly longer than what would be needed if manoeuvring just outside  $L_2$ .

The evolution of the minimum  $\Delta V$  conditions in Figure 6 takes a parabolic-like shape as  $\theta$  evolves, other than a few points for which the global minimum is found for high  $t_{\Delta v_2}$  values.

To visualise the distribution of the conditions such that the total  $\Delta V$  is minimum along the manifold trajectories, it is chosen to plot them in the rotating EM reference frame, from the points where the time spent by the spacecraft on the manifold is zero, to the point where  $t_{\Delta v_2}$  corresponds to a minimum  $\Delta V$  for a certain value of  $\theta$ . To ease the visualization overly complex, the total time considered is limited, minimum  $\Delta V$  conditions are computed a second time within this time frame, and the colour map that relates them to a certain value of  $\theta$  is appropriately rescaled. The resulting conditions, which can be identified in the left side of Figure 8, are shown as trajectories in the EM rotating frame on the right side of the same Figure.

In the right side of Figure 8,  $L_2$  is represented with a red dot. In blue, the ZVCs of the EM system for  $JC = JC_{L_2}$  are shown. The red area represents the ZVCs of the SE system for  $JC = JC_{SE-L_2}$ , where  $JC_{SE-L_2}$  is the  $JC$  of SE system at SE  $L_2$ . It is important to note that the rep-

resentation is purely qualitative, as the EM system rotates when the SE system is considered fixed, and vice versa. This means that the condition depicted is valid only at a specific instant. However, the ZVCs of the SE system are shown to provide an idea of the distances reached by the disposal trajectories. It is also reasonable to assume that once a certain distance from the barycentre of the EM system is reached, the approximation adopted by the CR3BP dynamics is no longer valid. Under these conditions, the inclusion of the Sun's gravitational influence in the system becomes necessary to approximate the dynamics with acceptable accuracy. However, all the solutions found are considered here to perform a complete analysis of the dynamics of  $L_2$  escape no-return disposal trajectories. The influence of the Sun will be added to the system in future work.

Trajectories in Figure 8 assume a spiral-like shape, distancing from the centre of the rotating system as the time corresponding to the minimum  $\Delta V$  manoeuvre increases. However, it is still difficult to identify why some minimum  $\Delta V$  conditions are at  $t_{\Delta v_2}$  greater than others as  $\theta$  varies. Disposal trajectories are shown in the Earth-centred rotating reference frame in Figure 9.

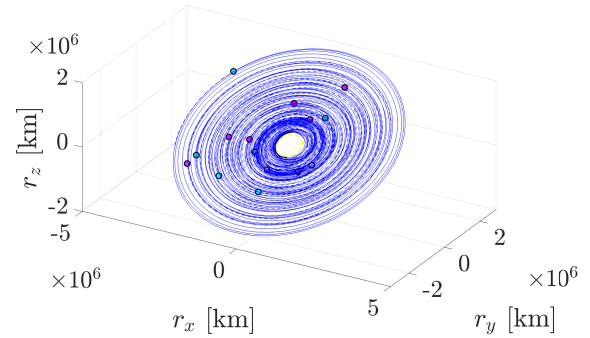


Figure 9: Trajectories corresponding to minimum disposal  $\Delta V$  conditions in the Earth-centred inertial reference frame. Halo  $L_2$ ,  $JC = 3.1383$ .

It is important to note that only some trajectories are shown in Figure 9, to enable the visualization of the dis-

tribution of conditions such that the disposal  $\Delta V$  is minimal.

In Figure 9, the solid blue lines are related to manifold trajectories before the lowest-cost disposal condition, and the dashed blue lines to manifold trajectories after the lowest-cost disposal condition. The trajectory of the Moon is represented as a yellow solid line. Note that the colours of the dots are chosen as for the colour map related to  $\theta$  and defined in Figure 3. Looking at this plot, it can be observed that the conditions such that the  $\Delta V$  required for disposal is minimum seem to correspond to those such that the distance between the Earth and the satellite travelling along the manifold is maximum. This quantity is consequently shown as a function of the time of flight spent by the spacecraft on the manifold in Figure 10.

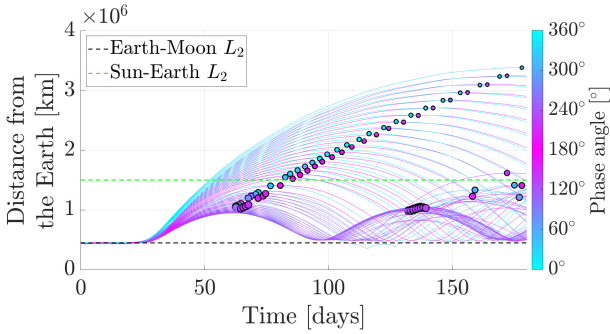


Figure 10: Evolution of the distance between the manifold and the Earth as a function of the time of flight spent by the satellite along the unstable manifold and the phase angle. Halo  $L_2$ ,  $JC = 3.1383$ .

In Figure 10, the dots represent the minimum  $\Delta V$  disposal conditions. The size of the dots is a function of how small or large the minimum  $\Delta V$  required to dispose of the spacecraft is out of the total of those considered as  $\theta$  varies. Two relevant behaviours can be observed. First, the minimum  $\Delta V$  conditions are always found when the satellite is at the apogee of the manifold. Secondly, the disposal cost is generally lower when the apogee of the manifold is higher, even if this second condition is not always verified.

Finally, one minimum disposal  $\Delta V$  trajectory is propagated after disposal in both the EM CR3BP and the  $n$ -body model for 100 years, as shown in Figure 11.

For the sake of brevity, only the results of the propagation of one condition are shown, but the findings reported are similar to the majority of those analysed. The trajectory after disposal, when propagated in the EM CR3BP, remains outside of the ZVCs for the entire time considered, following a predictable behaviour. As for the trajectory propagated in the  $n$ -body model, it appears that the impulse applied to close the ZVCs at  $L_2$  pushes the spacecraft away from cislunar space, preventing its reentry for up to 100 years. Given this behaviour, it is reasonable to assume that, in an  $n$ -body model, similar results could be achieved with lower values of  $\Delta v_2$ , at least under certain conditions. Consequently, this claim would only be confirmed by more complete simulations, performed in the

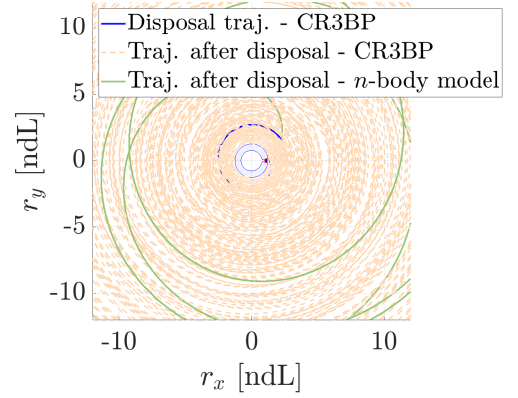


Figure 11: Trajectory after disposal, propagated in both the EM CR3BP and the  $n$ -body model. Halo  $L_2$ ,  $JC = 3.1383$ .

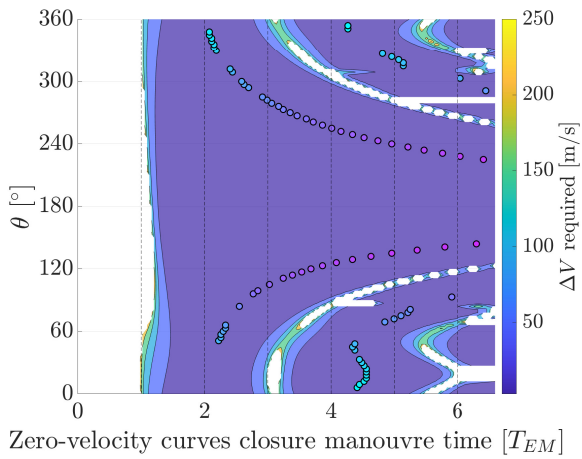
$n$ -body dynamical model.

In Figure 12, the disposal  $\Delta V$  as a function of phase angle and  $t_{\Delta v_2}$  is shown for all the orbits listed in Table 1.

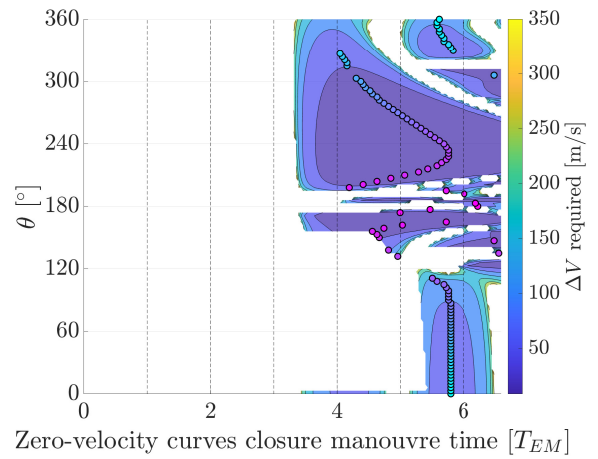
When there is a red area in the graphs, it indicates the manifold impacts on the Moon before exiting  $L_2$ . The green areas refer to the manifold trajectories that remain in cislunar space for the entire 6 months period without leaving the inner region of the ZVCs. No manifold trajectories impacting the Earth before exiting  $L_2$  were detected. It is interesting to note that the parabolic shapes defining the conditions for minimum disposal  $\Delta V$  are not centred at the same value of  $\theta$  for all members of a considered family. Intuitively, one might expect symmetry in disposal costs with respect to  $\theta = 0$  or  $\theta = 180$ , given that periodic orbits are symmetric about the  $xz$ -plane (or the  $x$ -axis in the planar case). However, this symmetry is not observed for all orbits analysed. The same applies to the distance between the orbit and the Moon, which, as shown earlier, varies closely as  $\theta$ . Since the trends of these two quantities are similar, it can be concluded that the disposal cost does not depend on both parameters in a similar way for all members of the considered families. As expected, disposal is more challenging for orbits around  $L_1$ , where, as shown in the figures, there are more impacts on the Moon or trajectories that remain in cislunar space. Conversely, the disposal becomes easier as the analysed orbit moves farther from the Moon along the family, i.e. as the mean distance between the orbit and the Moon increases. All other analyses are not reported for all the orbits considered, for the sake of brevity. Anyway, the results are consistent across all scenarios considered, allowing the conclusions drawn to be extended to all the orbits described in Table 1. Just as another example, the distance evolution for a Halo orbit in  $L_1$  is reported in Figure 13

## 5. CONCLUSIONS AND FUTURE WORKS

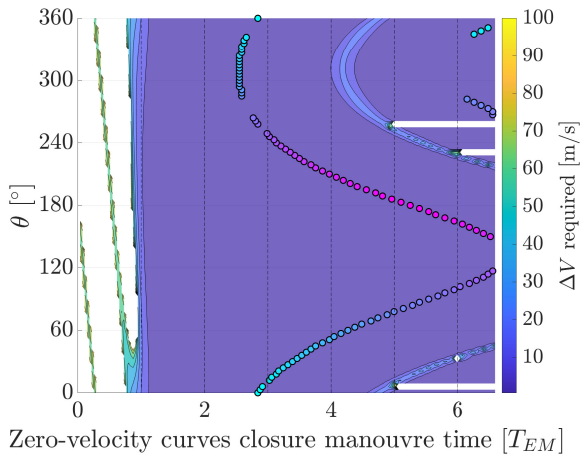
In this paper, the dynamics of EoL disposal for  $L_2$  escape no-return trajectories have been analysed. The disposal



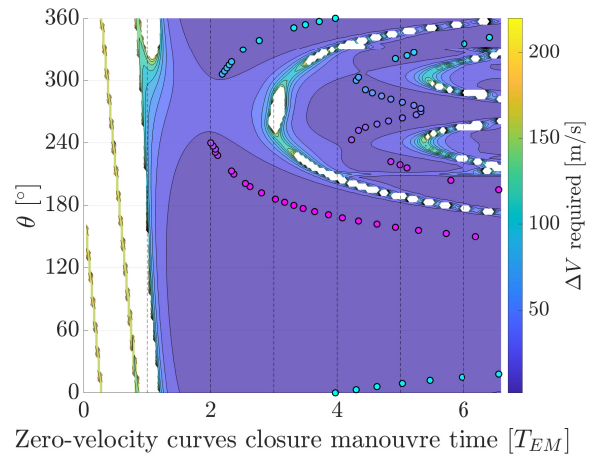
(a) Halo  $L_2$  -  $JC = 3.0988$ .



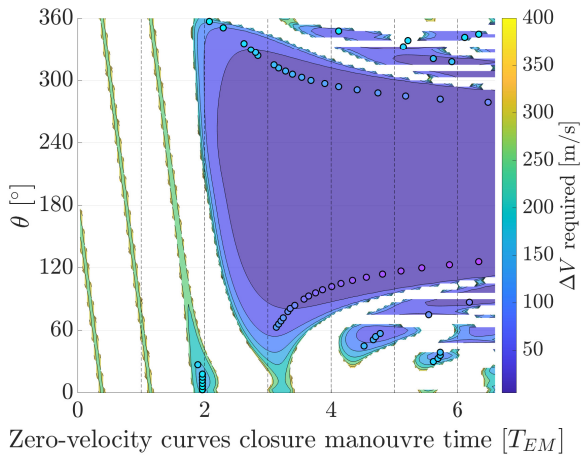
(b) Halo  $L_2$  -  $JC = 3.0289$ .



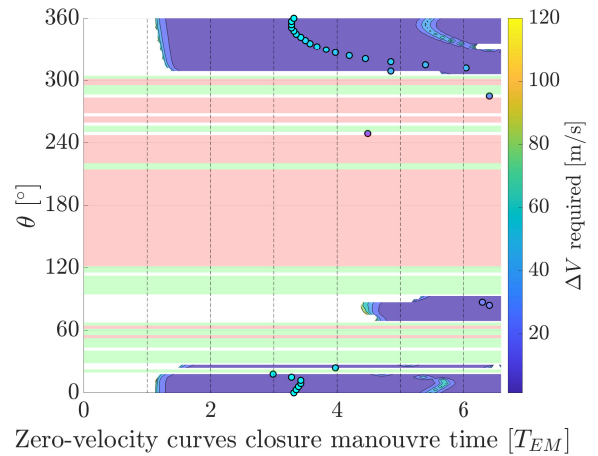
(c) Lyapunov  $L_2$  -  $JC = 3.1612$ .



(d) Lyapunov  $L_2$  -  $JC = 3.1161$ .

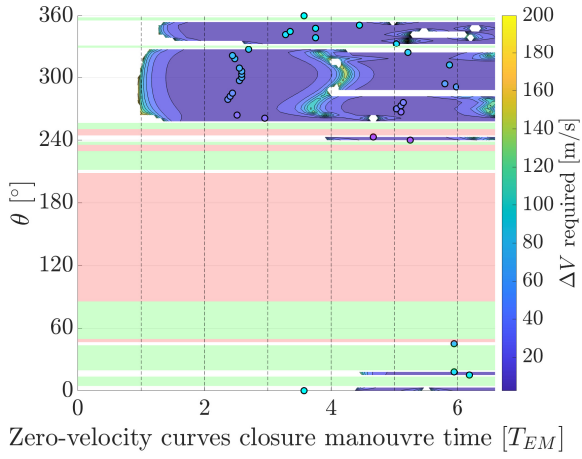


(e) Lyapunov  $L_2$  -  $JC = 2.9867$ .

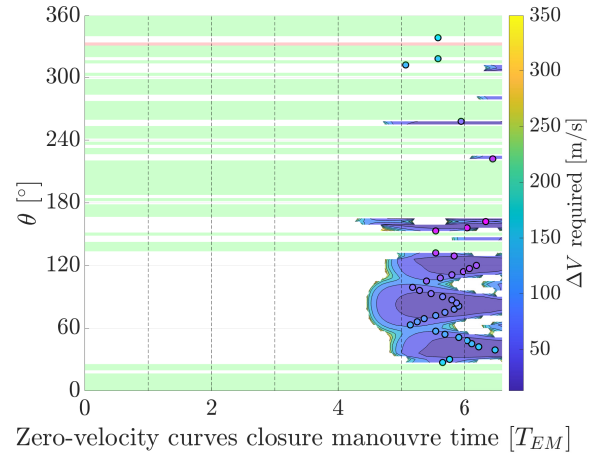


(f) Halo  $L_1$  -  $JC = 3.1525$ .

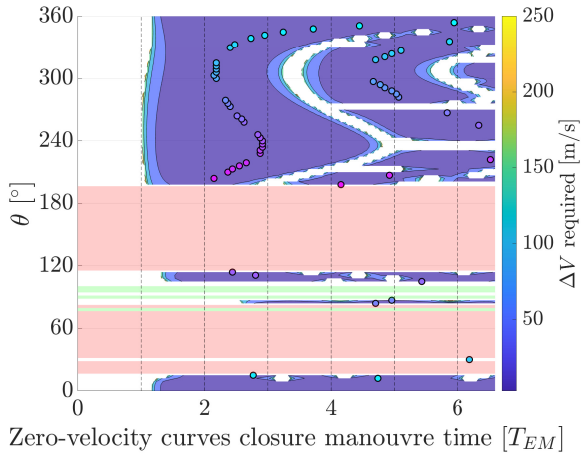
Figure 12: Disposal  $\Delta V$  as a function of phase angle and time the satellite spends on the manifold before performing the second disposal manoeuvre.



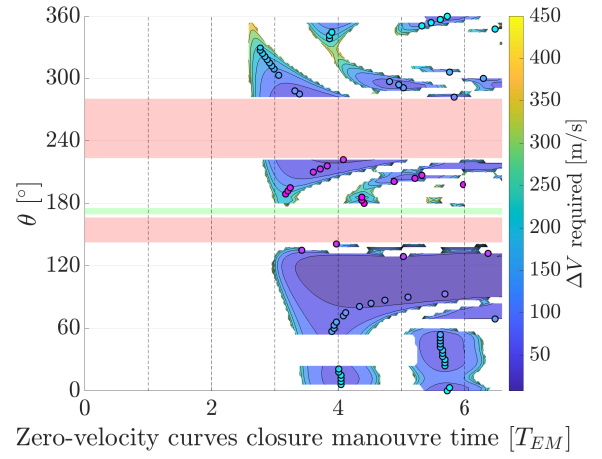
(g) Halo  $L_1$  -  $JC = 3.1239$ .



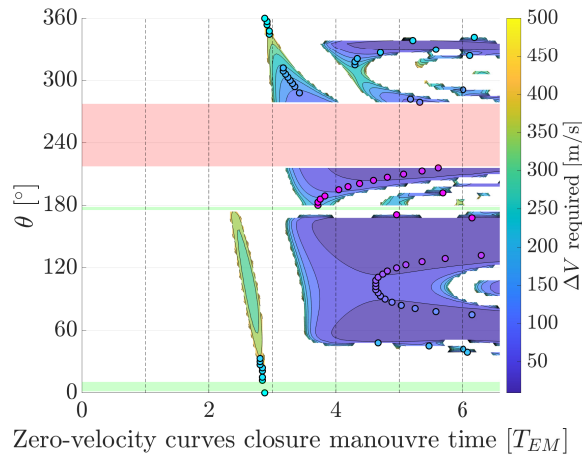
(h) Halo  $L_1$  -  $JC = 3.0025$ .



(i) Lyapunov  $L_1$  -  $JC = 3.0804$ .



(j) Lyapunov  $L_1$  -  $JC = 2.9370$ .



(k) Lyapunov  $L_1$  -  $JC = 2.8968$ .

Figure 12: Disposal  $\Delta V$  as a function of phase angle and time the satellite spends on the manifold before performing the second disposal manoeuvre.

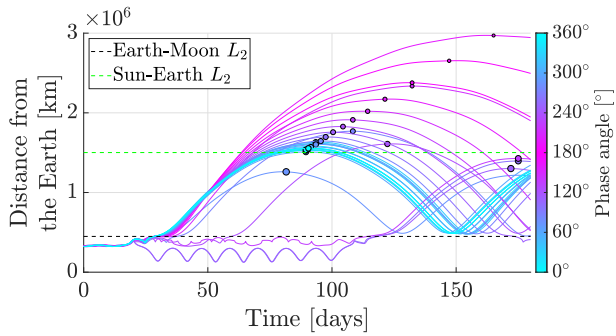


Figure 13: Evolution of the distance between the manifold and the Earth as a function of the time of flight spent by the satellite along the unstable manifold and the phase angle. Halo  $L_1$ ,  $JC = 3.11525$ .

cost has been examined as a function of various parameters, and it has been verified that, for some disposal trajectories, they remain outside the EM system for 100 years after disposal, both when propagated in the CR3BP and in an  $n$ -body dynamical model.

It was observed that the disposal cost, as a function of the phase angle, is minimized when the disposal trajectory reaches its apogee.

Additionally, disposal is less challenging for orbits around  $L_2$  than for those around  $L_1$ , as well as for orbits with a greater average distance from the Moon. Anyway, even for orbits in  $L_1$  where a high probability exists of impacting the Moon or remaining in cislunar space for many values of the phase angle, it is still possible to identify regions where disposal could be easy and fast to implement, making it a viable option.

As future work, we propose extending this analysis by first considering the Bicircular Restricted Four-Body Problem (BCR4BP) to account for the Sun's influence on the system and then moving to an  $n$ -body dynamical model to apply to the overall analysis, not only for validation. Regarding the latter, it would be of particular interest to assess how many of the trajectories propagated in the  $n$ -body model manages to avoid re-entering  $L_2$  for 100 years after disposal is performed.

Additionally, the analysis presented herein should be extended to trajectories that not only exit EM- $L_2$  but also SE  $L_2$ . Once there, the ZVCs of the SE system should be closed, just as demonstrated for the EM ones, to make it theoretically impossible for the satellite to return. Finally, the parametric analysis conducted in this study could be extended to other LPOs characteristics, such as the stability index, finite-time Lyapunov exponents, and more.

## ACKNOWLEDGEMENTS

This research has received funding as part of the work developed for the agreement n. 2023-37-HH.0 for the project "Attività tecnico-scientifiche di supporto a C-SSA/ISOC e simulazione di architetture di sensori per SST", established between ASI, Italian Space Agency, and POLIMI, Politecnico di Milano.

## REFERENCES

1. "NASA Artemis," available: <https://www.nasa.gov/feature/artemis/>. Last accessed: 24-03-2025.
2. "ESA'S annual space environment report," Tech. rep., ESA, ESOC, 2024, No. GEN-DB-LOG-00288-OPS-SD, [https://www.sdo.esoc.esa.int/environment\\_report/Space\\_Environment\\_Report\\_latest.pdf](https://www.sdo.esoc.esa.int/environment_report/Space_Environment_Report_latest.pdf).
3. "Process for limiting orbital debris," Tech. rep., NASA Standards, 2021, available: <https://standards.nasa.gov/sites/default/files/standards/NASA/C/0/nasa-std-871914c.pdf>.
4. "ESA Space Debris Mitigation Requirements," Tech. rep., ESA Space Debris Mitigation Working Group, 2023, Available: ESA Space Debris Mitigation Requirements.
5. Holzinger, M. J., Chow, C. C., and Garretson, P., "A primer on cislunar space," Tech. rep., Air Force Research Laboratory Greene County, OH, USA, 2021.
6. Olikara, Z. P., Gómez, G., and Masdemont, J. J., "Dynamic mechanisms for spacecraft disposal from Sun-Earth libration points," *Journal of Guidance, Control, and Dynamics*, Vol. 38, No. 10, 2015, pp. 1976–1989, doi: 10.2514/1.G000581.
7. Armellini, R., Rasotto, M., Di Lizia, P., and Renk, F., "End-of-life disposal of libration point orbit missions: The case of Gaia," *Advances in Space Research*, Vol. 56, No. 3, 2015, pp. 461–478, doi: 10.1016/j.asr.2015.03.014.
8. Colombo, C., Letizia, F., Soldini, S., and Renk, F., "Disposal of Libration point orbits on a heliocentric graveyard orbit: the GAIA mission," *Proceedings of the 25th International Symposium on Space Flight Dynamics (ISSFD)*, Munich, Germany, October 2015.
9. Colombo, C., Alessi, E. M., Van der Weg, W., Soldini, S., Letizia, F., Vetrivano, M., Vasile, M., Rossi, A., and Landgraf, M., "End-of-life disposal concepts for Libration Point Orbit and Highly Elliptical Orbit missions," *Acta Astronautica*, Vol. 110, 2015, pp. 298–312, doi: 10.1016/j.actaastro.2014.11.002.
10. Soldini, S., *Design and control of solar radiation pressure assisted missions in the sun-earth restricted three-body problem*, Ph.D. thesis, University of Southampton, Faculty of Engineering and the Environment, 2016.
11. Boudad, K. K., *Disposal dynamics from the vicinity of near rectilinear halo orbits in the Earth-Moon-Sun system*, Master's thesis, Purdue University, 2018.
12. Szebehely, V., *Theory of Orbit: The restricted problem of three Bodies*, Academic Press, 1st ed., 1967.
13. Doedel, E. J., Romanov, V. A., Paffenroth, R. C., Keller, H. B., Dichmann, D. J., GalÁN-Vioque,

- J., and Vanderbauwhede, A., “Elemental periodic orbits associated with the libration points in the circular restricted 3-body problem,” *International Journal of Bifurcation and Chaos*, Vol. 17, No. 08, 2007, pp. 2625–2677, doi: 10.1142/S0218127407018671.
14. Koon, W. S., Lo, M. W., Marsden, J. E., and Ross, S. D., *Dynamical Systems, the Three-Body Problem and Space Mission Design*, Marsden Books, 2011.
  15. Hénon, M., “Exploration numérique du problème restreint. II. Masses égales, stabilité des orbites périodiques,” *Annales d’Astrophysique*, Vol. 28, p. 992, Vol. 28, 1965, pp. 992.
  16. Battin, R. H., *An introduction to the mathematics and methods of astrodynamics*, Aiaa, 1999.
  17. “NASA SPICE,” available at: <https://naif.jpl.nasa.gov/naif/aboutspice.html>. Last accessed: 24-03-2025.